Characterization of the dynamic mechanical properties of low-iron float glass through Split-Hopkinson-Pressure-Bar tests

Characterization of the Dynamic Mechanical Properties of Low-iron Float Glass through Split-Hopkinson-Pressure-Bar Tests

Xing Chen [2], Changzhong Wang [2], Suwen Chen [1, 2 *], Siyi Yi [2], and Yong Lu [3]

1 State Key Laboratory for Disaster Reduction in Civil Engineering, Tongji University, Shanghai 200092, China.

2 College of Civil Engineering, Tongji University, Shanghai 200092, China.

3 School of Engineering, The University of Edinburgh, Edinburgh EH9 3JL, UK.

Abstract

Low-iron ultra-clear float glass (LIFG) has been widely used in landmark and large-scale buildings in recent years due to its aesthetic characteristics. A better understanding of the dynamic mechanical properties of LIFG is essential for the blast resistance analysis and design of glass facades. This paper presents a series of quasi-static tests and dynamic tests (using Split-Hopkinson-Pressure-Bar) to study the dynamic compressive and tensile behavior of LIFG. Strain rate effect has been investigated on compressive strength in the range of 10^{-5} s^{-1} to 10^{3} s^{-1} and splitting tensile strength in the range of 10^{-5} s^{-1} to 40 s^{-1}. During the tests, an ultra-high-speed camera was employed to capture the crack initiation and propagation. The test results show that both the dynamic compressive and tensile strengths of LIFG are strain-rate dependent, nevertheless the dynamic tensile strength is more sensitive to strain rate than the compressive strength. The strain rate effect is insignificant on the Young's modulus of LIFG. In addition, the upper limits of strain rate are identified for dynamic

compression and splitting tension of glass through SHPB facilities based on a conceptual analysis. For LIFG specimens with the length of 8 mm (for compression) or the diameter of 20 mm (for splitting tension), the upper limit of strain rate is about 2500 s^{-1} for compression and about 40 s^{-1} for splitting tension. Increasing or reducing the specimen dimension will correspondingly decrease or increase the upper strain rate limits.

Keywords: Low-iron float glass (LIFG), strain rate, Split-Hopkinson-Pressure-Bar (SHPB), dynamic mechanical property, dynamic increase factor (DIF)

1. Introduction

Glass, a non-crystalline amorphous solid, has been widely used for facades of modern buildings as it is transparent and can provide outstanding aesthetical effect. However, due to glass's brittle nature, glass facade may fracture into high-speed shards in impact or blast loading and cause serious injuries. For example, in the event of 1995's Murrah Federal Building Car Bombing in Oklahoma USA, over 40% injuries were related to high-speed flying glass shards [1]. This event and several other bombing attacks have shown that high-speed flying glass fragment is one of the key factors responsible for human casualties in bombing attacks. Therefore, it is of great importance to investigate the dynamic response and blast resistance of glass facade. Establishing the dynamic properties of glass, which is the focus of this paper, provides the basis for researches in this topic.

The properties of glass are mainly affected by the chemical components and manufacture techniques. Silica (SiO_2) is a common fundamental constituent of glass. According to its ingredients, silicate glasses can be classified as fused silica, soda-lime-silica glass, borosilicate glass, aluminosilicate glass and so on. Float glass, mostly made of soda-lime-silica glass, is a sheet of glass panel produced by floating molten glass on a bed of molten metal, typically tin. Low-iron float glass (LIFG), also named as ultra-white glass or ultra-clear float glass, is a type of high-clarity glass made from low-iron silica sand, in which the ferric oxide content can be as low as 0.01% or one tenth of that in soda-lime-silica glass. The chemical compositions of the glass used in this study are listed in Table 1 in comparison with those reported in other studies in the open literatures. It can be observed that the proportion of iron in LIFG is significantly lower than other types of glass. This low level of iron leads to less absorption of green and purplish red bands in visible light and results in better consistency of glass color, higher light-transmittance and better transparency. Therefore, LIFG has been a favorable choice by architects, especially for landmark buildings, such as the Louvre Pyramid (France), Shanghai Tower (China), Burj Khalifa Tower (Dubai) and so on.

Table 1 Chemical compositions of different types of silicate glass

Source	Test material	Percentage of chemical composition (%)						
Holmquist et al. [2]	Annealed float glass	SO_2	Na_2O	CaO	MgO	Al_2O_3	K_2O	Fe_2O_3
		73.7	10.6	9.4	3.1	1.8	1.1	0.2
Nie et al. [3]	Borosilicate glass	SO_2	Na_2O	B_2O_3	Al_2O_3			
		80.5	3.5	12.7	2.5			
Li et al. [4, 5]	Annealed float glass	SO_2	Na_2O	CaO	Al_2O_3	K_2O	Others	
		72.5	13.0	9.3	1.5	0.3	3.4	
Peroni et al. [6]	Low-iron float glass	SO_2	Na_2O	CaO	MgO	Al_2O_3	K_2O	Fe_2O_3
		72.7	13	8.8	4.3	0.6	0.4	0.02
Zhang et al. [7, 8]	Annealed float glass	SO_2	Na_2CO_3	Cullet	$CaMg(CO_3)_2$	$CaCO_3$	Others	
		51	16	15	13	4	1	
Daryadel et al. [9]	Fused silica	SO_2	Others					
		>99	<1					
	Soda-lime	SO_2	Na_2O	CaO	Al_2O_3	Fe_2O_3	Others	
		72	14.2	10	0.6	0.1	2.5	
	Borosilicate	SO_2	Na_2O	Al_2O_3	B_2O_3	Others		
		81	4.5	2	12	0.5		
	Starphire	SO_2	Na_2O	CaO	Others			
		73	14	10	3			
Sheikh et al.		SO_2	CaO	Al_2O_3	B_2O_3	MgO	BaO	

[10-12]	Aluminosilicate glass	57	10	16	4	7	6		
Meyland et al.[13]	Annealed float glass	SO_2	CaO	Na_2O	MgO	Al_2O_3	Others		
		74	8.5	12.8	4.0	0.5	0.2		
Current study	Low-iron ultra-clear glass	SO_2	Na_2O	CaO	MgO	Al_2O_3	K_2O	Fe_2O_3	SO_3
		72.2	14.3	6.4	4.3	1.2	1.2	0.03	0.30

Note: The chemical compositions of the glass used in this study were provided by the manufacturer.

The static mechanical properties of glass have been intensively studied, mainly through four-point bending test or coaxial double ring (CDR) test [14-16]. It is understood that the fracture of glass is probabilistic due to the existence of micro-cracks and defects, and its fracture strength can be generally characterized by Weibull distributions [15-17]. The dynamic mechanical properties of glass are of great interest when glass is exposed to impulsive loading such as impact and blast loading. To investigate the mechanical properties of different types of silicate glass under dynamic loadings, quite a few dynamic compression and splitting tensile tests have been conducted using Split Hopkinson Pressure Bar (SHPB) systems. Together with high-speed cameras, the crack initiation and failure process can be captured. Existing studies show that silicate glass normally behaves linear elastically and exhibit brittle failure under both quasi-static and dynamic loadings, and strain rate effects can be observed in the failure strengths [2, 4-9, 11-13, 18, 19]. The strain rate effects are mainly due to the fact that multiple micro-cracks are triggered under dynamic loading before fracture, and the initiation and propagation of micro-cracks need time [11]. Previous studies also indicate that the strain rate sensitivity of silicate glass differs in compression and tension. For example, Peroni et al. [6] concluded that high purity optical glass (low-iron float glass) does not exhibit any substantial sensitivity to the strain rate in the ultimate compressive strength, but the tensile strength can increase by about 60% when the strain rate rises to six orders of magnitude from a quasi-static baseline. Similarly, Sheikh et al. [11] found that the dynamic increment in the splitting tensile strength of aluminosilicate glass is more significant comparing to compression. Despite these observations, the mechanisms that lead to the difference between compressive and tensile strain rate sensitivities are still an open question. Moreover, the strain rate effect is found to be insignificant on the Young's modulus in both compression and tension [6, 7].

In general, different strain rate effects have been reported different types of silicate glass. However, only very limited experimental results are reported in open literatures when considering strain rate beyond 10^0 s^{-1}. The existing test results have not yielded a clear conclusion about the strain rate sensitivity of silicate glass. Besides, silicate glass with different chemical compositions may exhibit different dynamic mechanical properties, but so far there has been very limited research on the strain rate properties of low-iron float glass. Only Peroni et al. [6] conducted dynamic tests on LIFG, but they did not record the glass strain or strain rate in the splitting tensile tests. Therefore, more dynamic tests are necessary to better understand the strain rate properties of LIFG.

This paper presents a comprehensive experimental study on the dynamic mechanical properties of LIFG. A series of static and dynamic tests were carried out using an electronic universal testing machine and SHPB to investigate the strain rate effects on the compressive and splitting tensile properties of LIFG. For the splitting tests, the splitting pattern was captured using a synchronized ultra-high-speed camera. The stress equilibrium has been carefully checked to ensure the validity of the dynamic test data. Based on the test results, key mechanical parameters, such as the ultimate strength and ultimate strain, as well as the Young's modulus, were obtained from for both splitting tensile and compressive cases. Finally, the dynamic increase factors (DIFs) of both splitting tensile strength and compressive strength are suggested for possible applications in the blast resistant analysis and design of glass facades involving LIFG.

2. Quasi-static tests

2.1 Test method

A series of quasi-static compression and splitting tensile tests (also known as Brazilian test) were conducted first to study the basic static mechanical properties of LIFG. The test specimens for all tests were taken from LIFG provided by Hangzhou Yuhong Technology Co., LTD. According to the information from the manufacturer, the glass has a mass density of 2.479 g/cm^3, a coefficient of expansion of 90.8×10^{-7} /°C and a Poisson's ratio of 0.21, and its chemical composition is listed in Table 1. The test specimens were all in a cylindrical shape but differed in dimensions. The geometries of the specimens for quasi-static tests and dynamic tests are detailed in section 2.1 and section 3.1, respectively. All specimens were cut from intact glass plates and carefully polished to avoid initial imperfection on the edges. For each cylindrical specimen, the two end faces were ensured to be parallel with a tolerance within 0.2 mm, mainly to avoid undesirable fracture mode resulting from geometric imperfection [20].

The quasi-static tests were carried out at Northwestern Polytechnical University (in China) with an electronic universal testing machine DNS-100 (Fig. 1a), which has a loading capacity of 100 kN. The test temperature was 22±2 °C and the relative air humidity was 50±5%. The force was recorded by a built-in piezoelectric load sensor with a relative error of less than ±0.5%, and the sampling frequency was set to 10 Hz. A constant loading rate of 0.2 mm/min (speed of the loading end) was used for both compressive and splitting tensile tests (Table 2).

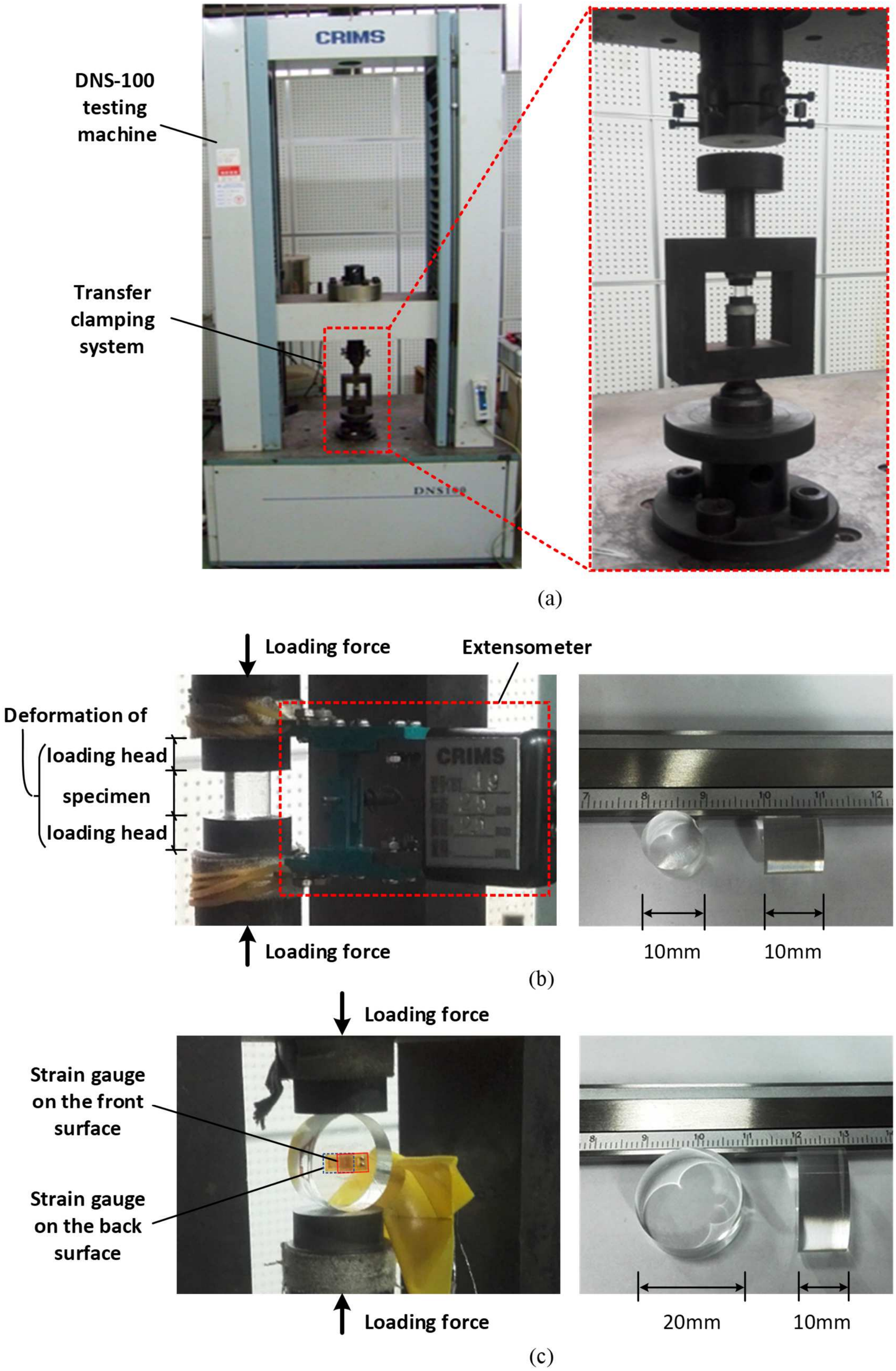

Fig. 1. Illustration of quasi-static tests: (a) loading machine, (b) measurement and specimen for compressive tests and (c) measurement and specimen for splitting tensile tests

As shown in Fig. 1b, the specimens for static compressive tests are cylinders of 10mm in height and 10mm in diameter. The deformation of glass cylinder was traced by an extensometer with a relative error of less than ±0.5%. The obtained displacement data from extensometer includes both the deformation of the specimen and the deformation of the loading heads within the measured section. To eliminate the deformation of the loading heads, preliminary compressive tests without glass specimen were conducted and the deformation of the loading heads was measured, which was then used as an approximation of the real deformation of the loading heads developed in the compressive test with glass specimen. Despite that in the above two cases the stress states of the loading heads (especially near the contact surfaces) are not exactly the same, this approach can mostly remove the deformation of the loading heads from the total deformation.

Table 2 Testing condition for static tests

Test type	Loading speed (mm/min)	Diameter (mm)	Thickness (mm)	Number of specimens
Static compressive test	0.2	10	10	6
Static splitting tensile test	0.2	20	10	5

Brazilian disc splitting tests were used to get the tensile strength for the glass. In a typical splitting tensile test, a concentrate line load P is applied to a Brazilian disc specimen, and the disc will be split into two halves along the diameter between the two loading points when the tensile stress exceeds the tensile strength. Fig. 2 shows a typical distribution of the horizontal stress for the specimen in a splitting tensile test, where a uniform horizontal tensile stress will be developed along the majority of the vertical central line with lateral compression in both top and bottom parts of the diameter [21]. Based on the plane-stress hypothesis, the splitting tensile strength σ_t can be calculated by Eq. 1 [21]. In the present study, glass discs of 20 mm in diameter and 10 mm in thickness (Fig. 1c) were used for splitting tensile tests. Two strain gauges were attached at the center of both surfaces to record the strain in the splitting direction until glass fracture.

$$\sigma_t = \frac{2P}{\pi DB} \tag{1}$$

where P is the load applied on the disc, and D and B are the diameter and thickness of the disc respectively, as shown in Fig.2.

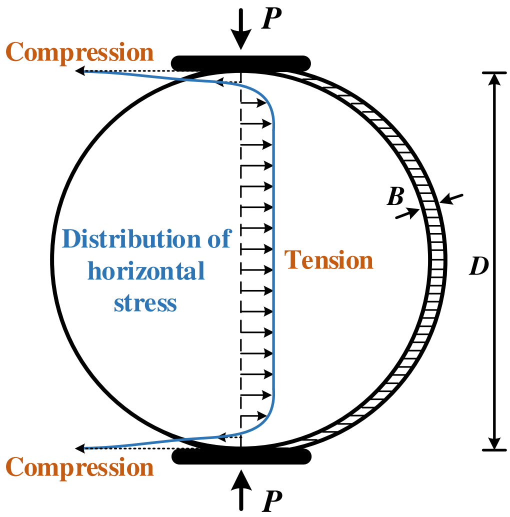

Fig. 2 Schematic illustration of the quasi-static splitting test

2.2 Test results

2.2.1 Quasi-static compressive test

Fig. 3 shows the crack pattern of a specimen before fracture in both meso- and macro- scales. The corresponding load is about 90% of the maximum load. As shown in Fig. 3a and 3b, when the specimen is about to fracture, a narrow region of high crack density is formed as the cracks grow and interact. These shaggy and irregular cracks grow in an unstable manner and result in a macroscopic fracture plane (perpendicular to end surfaces) that leads to ultimate failure. The specimen was eventually crushed into fine powder with a tremendous sound. Compared to the final failure of normal float glass (NFG) as shown in Fig. 4b and 4c, the fragments from the LIFG is far finer than that of the NFG. This indicates that the LIFG material has far less initial imperfection and could fractured more uniformly than the NFG, which may lead to a higher compressive strength.

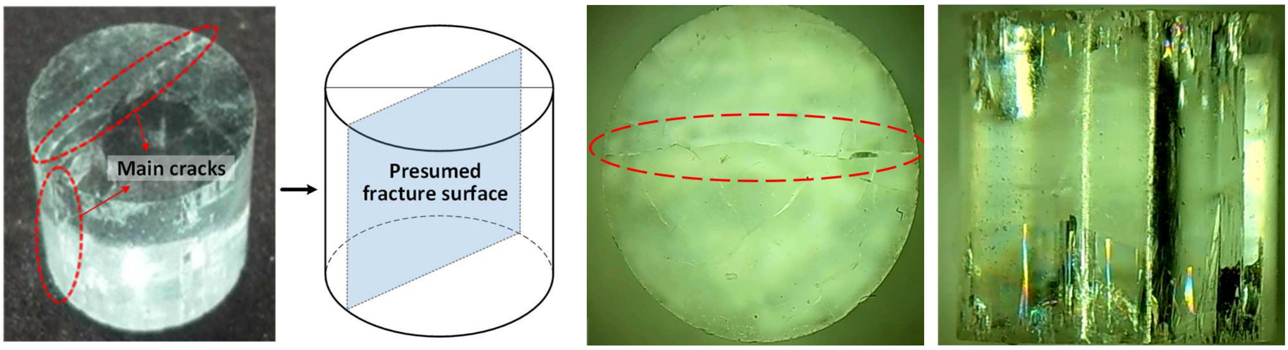

(a) (b) (c)

Fig. 3 Experimental phenomena before failure (at around 90% of the maximum load): (a) Specimen before fracture and presumed fracture surface, (b) Front view of cracks and (c) Side view of cracks

(a) (b) (c)

Fig. 4 Comparison of glass fragments after quasi-static compressive tests: (a) the LIFG in current study (compressive strength ≈ 1038 MPa), (b) NFG (compressive strength ≈ 767 MPa) [22], and (c) NFG (compressive strength ≈ 256 MPa) [7]

The obtained Eng. stress- Eng. strain curves are presented in Fig. 5. The Eng. stress was calculated by dividing the measured force by the original sectional area of the specimen. The Eng. strain was calculated by dividing the deformation of the specimen, which equals to the total cross-head movement measured by the extensometer minus the deformation of the loading heads, by the original length of specimen. As can be seen in Fig. 5, the LIFG behaves almost linear elastically up to fracture. No descending phase can be observed on the stress-strain relationships after the ultimate compressive strength is reached, indicating the failure of LIFG is very brittle. The 6 tested specimens have similar stiffness but exhibit large variation in the ultimate compressive strength and strain. This could be mainly due to the differences in the distribution and size of surface flaw among specimens. Based on the test results, the elastic modulus, ultimate compressive strength and ultimate compressive strain are determined for each test specimen and the results are summarized in Table. 3. The elastic modulus is taken as the average slope of the middle part (between 1/3 and 2/3 of the ultimate stress) of each stress-strain curve. The ultimate compressive strength and ultimate compressive strain correspond to the stress and strain at failure point, respectively. The compressive modulus is around 64 GPa. The average ultimate compressive strength is 1037.67 MPa with a standard deviation of 179.28 MPa, while the average strain is 1.77% with a standard deviation of 0.26%.

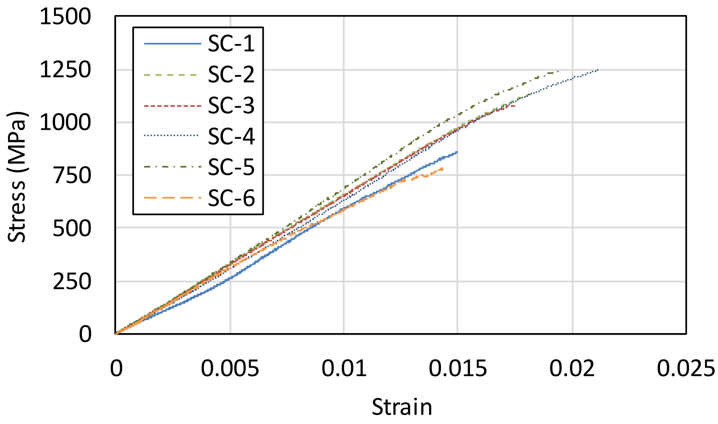

Fig. 5 Stress-strain curves for static compressive tests

Table 3 Results for static compressive tests

Specimen no.	Dimensions		Total deformation (mm)	Deformation of the loading heads (mm)	Ultimate strain	Ultimate stress (MPa)	Elastic modulus (GPa)	Strain rate ($\times10^{-5}$ s^{-1})
	Diameter (mm)	Thickness (mm)						
SC-1	9.94	9.88	0.20	0.05	1.50%	861.35	59.19	4.77
SC-2	9.78	10.02	0.24	0.06	1.84%	1140.09	65.69	5.09
SC-3	9.84	10.02	0.23	0.06	1.76%	1078.96	65.12	5.23
SC-4	9.70	10.02	0.28	0.07	2.12%	1119.49	62.49	5.52
SC-5	9.80	10.02	0.25	0.06	1.95%	1247.06	67.83	4.49
SC-6	9.84	10.02	0.19	0.05	1.44%	779.06	61.70	4.07
Average value			0.23	0.06	1.77%	1037.67	63.67	4.86
Standard Deviation			0.03	0.01	0.26%	179.28	3.13	0.53

2.2.2 Static splitting tensile test

Fig. 6 shows a typical failure mode of Brazilian splitting test. Due to the elastic-brittle property of the glass, the specimen split into two halves in such a sudden manner that it is difficult to observe the initiation and development of crack as shown in the compressive tests. The oval-shaped solid lines in Fig. 6 depict typical crack orientation, which appears to relate to the friction at the interface of specimen and loading head although the interface was well lubricated. The core area is fractured into tiny fragments. All specimens split into two halves just as predicted in the elastic theory and the glass tip of specimen near the loaded head is not crushed, which illustrates the validity of static splitting tests for the glass specimens.

(a) (b)

Fig. 6 Typical fracture pattern in static splitting tests (from SS-1): (a) fracture pattern and (b) fracture pattern microphotograph of fracture surface

The processed tensile stress-strain curves are presented in Fig. 7. The Eng. stress was calculated from the loading force based on Eq. 1, and the Eng. strain was measured by strain gauges. Similar to the results from compressive tests, the LIFG behaves almost linear elastically and fractured brittlely. As listed in Table 4, the average tensile strength for the tested glass is 29 MPa with a standard deviation of 5.14 MPa. The average tensile strength is only about 1/35 of the average compressive strength. The average failure strain is about 0.05% with a standard deviation of 0.008% and tensile modulus is around 64 GPa with a standard deviation of 3 GPa.

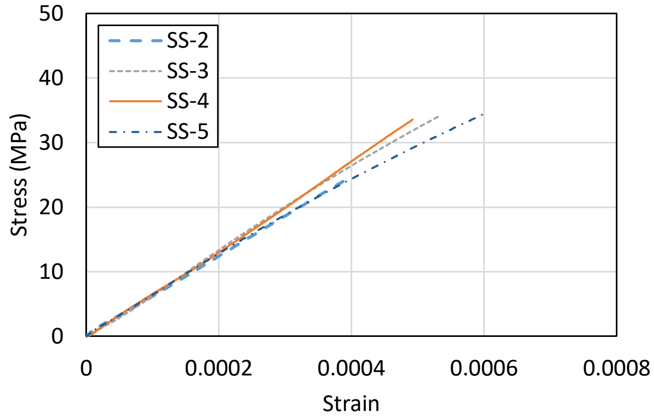

Fig. 7 Stress-strain curve for static splitting tensile tests

Table 4 Results for static splitting tensile tests

Specimen No.	Dimensions		Ultimate strain	Ultimate stress (MPa)	Elastic modulus (GPa)	Strain rate ($\times 10^{-5}$ s^{-1})
	Diameter (mm)	Thickness (mm)				
SS-1	19.86	9.2	—	23.03	—	—
SS-2	19.98	9.2	0.040%	24.51	62.51	1.30
SS-3	19.98	9.24	0.053%	33.88	65.62	1.80
SS-4	19.92	9.22	0.049%	33.57	66.92	1.30
SS-5	20.00	10.02	0.060%	31.37	60.28	1.70
Average value			0.050%	29.27	63.83	1.53
Standard deviation			0.008%	5.14	3.01	0.26

3. Dynamic tests

3.1 Test method and assumptions

The dynamic compression and splitting tensile tests were performed using the split Hopkinson pressure bar (SHPB), which is one of the most common techniques for studying the dynamic properties of materials. The SHPB facility can also be used together with Brazilian Disc samples to realize dynamic splitting tensile loading. A schematic illustration of the SHPB setup with a compressive sample is shown in Fig. 8a. In a SHPB test, the specimen is fixed between the incident bar and transmitter bar. A compressive stress wave will be generated from one end of the incident bar through the impact of a high-speed projectile (striker bar). The stress wave will propagate and pass through the specimen, and the specimen is loaded. The strain rate a specimen is experienced during the test is correlated with the amplitude of the incident stress wave, which can be adjusted by changing the launching velocity of the projectile.

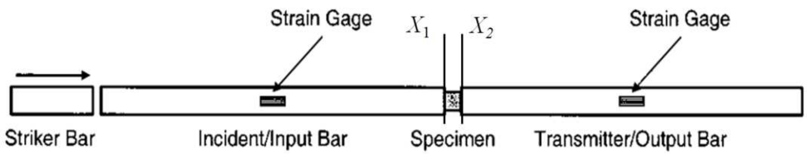

(a)

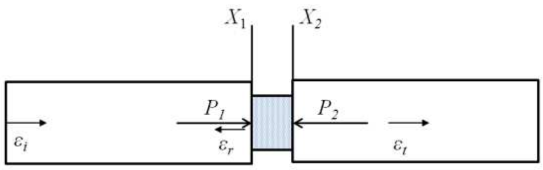

(b)

Fig. 8 Illustration of SHPB setup: (a) a sketch of SHPB setup with a compressive test specimen[23] and (b) one-dimensional stress wave propagation in SHPB

Two basic assumptions of the SHPB setup are: (1) 1-D linear elastic wave in the bars, which means uniform axial stress distribution in every cross section of bars; (2) Stress equilibrium has been reached in the test specimen. Strain gauges installed on the incident bar and the transmitted bar can record the incident wave, reflected wave and transmitted wave. The force acting on the two ends of the specimen can be calculated with the following equations:

$$P_1 = A_i E_i (\varepsilon_i + \varepsilon_r) \quad (2)$$

$$P_2 = A_t E_t (\varepsilon_t) \quad (3)$$

where P_1 and P_2 are forces acting on the specimen at the interfaces X_1 and X_2 shown in Fig. 8b, A_i and A_t are the cross-section area of the incident bar and the transmitted bar, E_i and E_t are Young's modulus of materials for the incident bar and the transmitted, and ε_i, ε_r and ε_t are the recorded strains of the incident wave, reflected wave and transmitted wave.

Assuming that the materials of both incident and transmitted bars are the same, the strain rate $\dot{\varepsilon}_{ic}$ and strain ε_{ic} of the test specimen can be calculated with the following equations:

$$\dot{\varepsilon}_{ic} = -\frac{2C_0}{L_s}\varepsilon_r \quad (4)$$

$$\varepsilon_{ic} = -\frac{2C_0}{L_s}\int_0^t \varepsilon_r \, dt \quad (5)$$

where L_s is the specimen length and C_0 is elastic wave speed in the bars.

For the dynamic compressive tests, Ø19mm bars made of martensitic steel (Young's modulus = 194 GPa) were used for the striker bar, incident bar and transmitted bar. The interfaces were lubricated to reduce friction. A copper pulse shaper was adopted to filter the high-frequency components within the incident wave. An ultra-high-speed camera SIMD8 produced by Specialized Imaging, shown in Fig. 9a, was used to capture the fracture process of the test specimen with intervals of 1ns to 5μs. The camera was synchronically triggered with the impact bullet.

A group of 16 specimens were tested to obtain the dynamic compressive property of the glass at three loading rates (Table 5). The specimens for the dynamic compressive tests were glass cylinders with a diameter of 8mm and a length of 6mm (Fig. 9b). Two strain gauges were attached to the cylindrical surface of each specimen to measure the strain in the loading direction. It is worth noting that the glass surface was slightly grinded in a local area in order to glue the strain gauge, and this is assumed to cause little influence on the compressive fracture strength since the ground area is quite small compared to total surface area. Three different air pressures, i.e., 0.1MPa, 0.15MPa and 0.2MPa, was used for the gas gun to obtain different impact velocity of the striker bar.

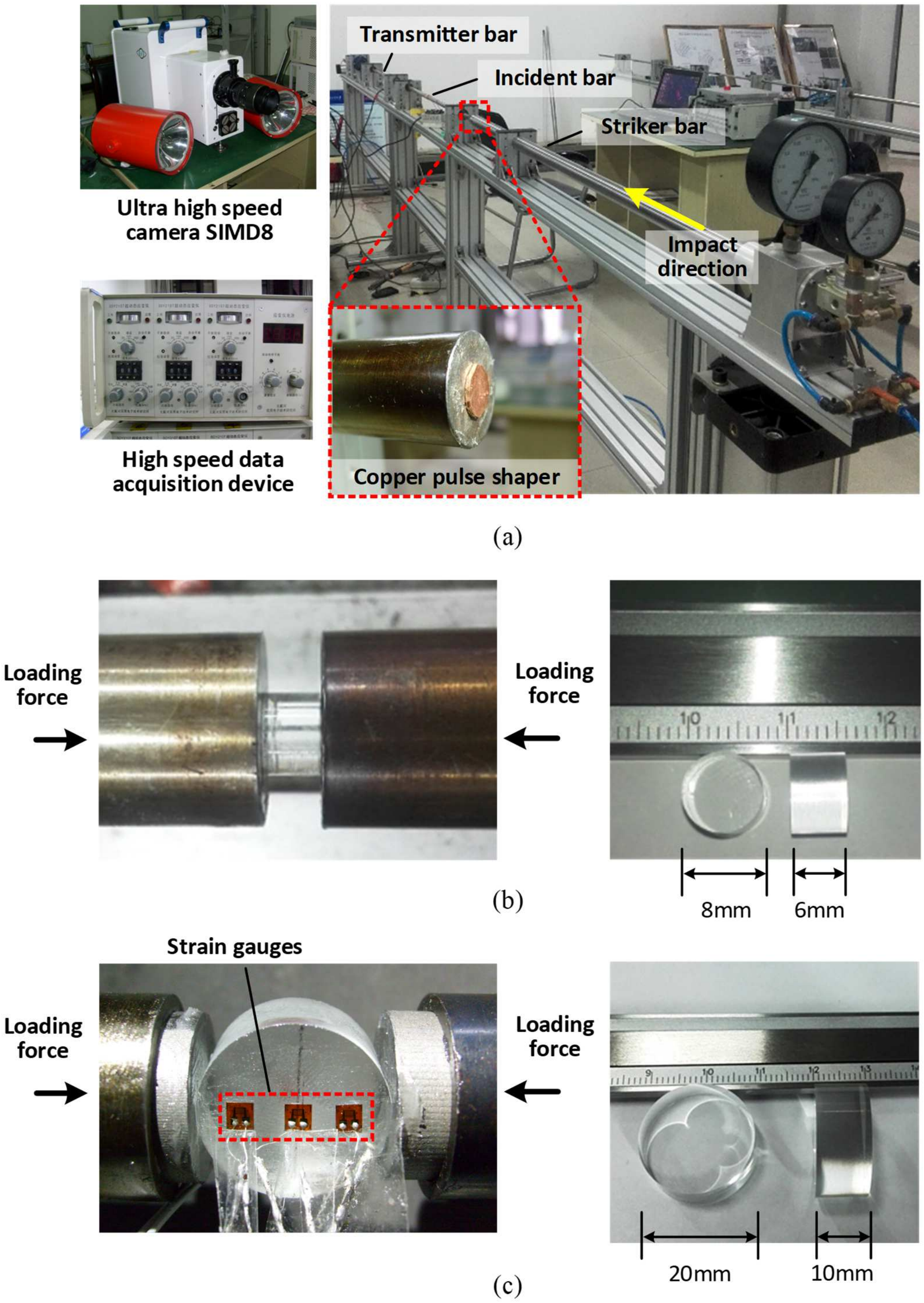

Fig. 9 Illustration of dynamic tests: (a) loading machine, (b) measurement and specimen for compressive tests and (c) measurement and specimen for splitting tensile tests

Table 5 Testing parameters for dynamic tests

Test type	Air pressure (MPa)	Diameter (mm)	Thickness (mm)	Number of specimens
Dynamic compressive test	0.1	8	6	6
	0.15			4
	0.2			6
Dynamic splitting tensile test	0.03	20	10	5
	0.05			6

Note: The air pressure was controlled by an internal pressure gauge with a relative error of ±1%.

In the present study, the SHPB apparatus was also employed to perform the dynamic splitting tensile tests, by loading the glass disc in the diameter direction with the SHPB (Fig. 10). For a dynamic splitting test, two key factors affecting the accuracy are stress equilibrium and shape effect of a sample. For brittle materials such as glass, ceramic and concrete, the specimen can easily break up before reaching a stress equilibrium. To overcome this issue, a pulse shaper made of copper or rubber is often used to modify the incident wave into a triangular wave. More detailed information about the pulse shaper can be found in literature [24]. Apart from this, a spindle projectile has been employed to shape the incident pulse into a half sine wave[7]. The second factor that might affect the test result is shape effect. It should be noted that the deduction of Eq. 1 is based on the assumption of plane stress, in which the influence of thickness is neglected. Yu et al. [25] have proposed a coefficient to modify the traditional 2-D equation. However, since the error from shape effect is much smaller compared with systematic error in the tests, Eq. 1 without modification is used to calculate tensile strength in this study.

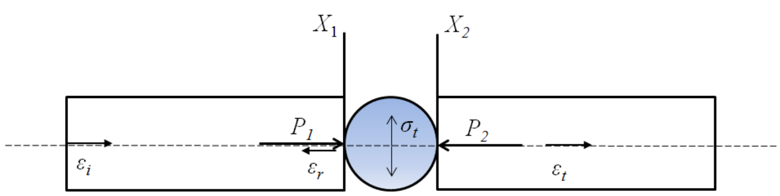

Fig. 10 Loading setup for splitting test with a Brazilian disc in SHPB

A total of 13 specimens with diameter of 20mm and thickness of 10mm were used for dynamic splitting tensile tests (Fig. 9c). Different from the dynamic compressive strength tests, an aluminum bar is adopted for the transmitted bar in the dynamic splitting tests to improve the signal-noise-ratio of the transmitted wave as the Young's modulus of aluminum (around 74GPa) is close to that of glass. To measure the strain in the splitting direction, each specimen was attached with a set of strain gauges on both flat faces along the central line, as shown in Fig. 9c. To ensure that a stress equilibrium is reached before glass fracture, a copper pulse shaper was attached to the end of striker bar to modify the shape of incident wave so that the incident wave rises less steeply. All the specimens were lubricated with Vaseline to reduce friction on the contact surfaces to minimize the friction effect.

3.2 Test results

3.2.1 Dynamic compressive test

Fig. 11 shows a typical fracture process of a specimen (DC-A-1) in a dynamic compressive test. The corresponding stress time-history is presented to provide a coupling to the high-speed images. In this case the pressure of air gun was 0.1 MPa. As can be seen, the specimen remained intact at first, and major cracks initiated almost simultaneously from the end surfaces of the glass disc at 205 μs. Then, dense cracks accumulated in the end region close to the incident bar, and several major longitudinal cracks as well as vertical cracks penetrated through the glass disc at 210 μs, leading to a noticeable decline in the compressive stiffness of the glass. More cracks developed and propagated throughout the entire specimen afterwards, and finally the specimen was crushed into glass powder at 225 μs.

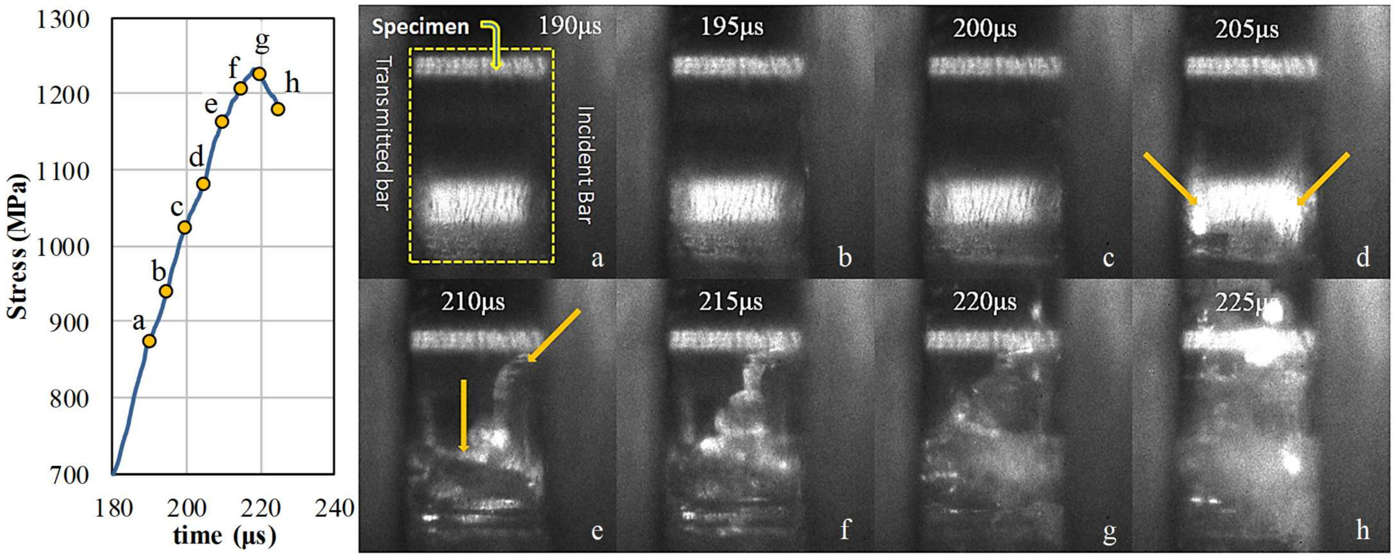

Fig. 11 Typical failure process in a dynamic compressive test (DC-A-1, initial air gun pressure = 0.1 MPa)

The strain signals from the incident bar and transmitter bar are carefully checked to ensure the dynamic equilibrium. As shown in Fig. 12, the incident wave has been effectively modified into a smooth triangular wave without sharp increase due to the copper pulse shaper. The plateau section of the reflected wave is related to loading on specimen and the rising part afterwards is the residual incident wave reflecting at the incident bar end. To illustrate the attainment of a dynamic equilibrium in the test specimens, the values of σ_i+σ_r and σ_t on the two bar-specimen interfaces are compared in Fig. 12 for three representative specimens (one for each air pressure). The two curves are basically overlaid after synchronization, indicating that the dynamic equilibrium was reached.

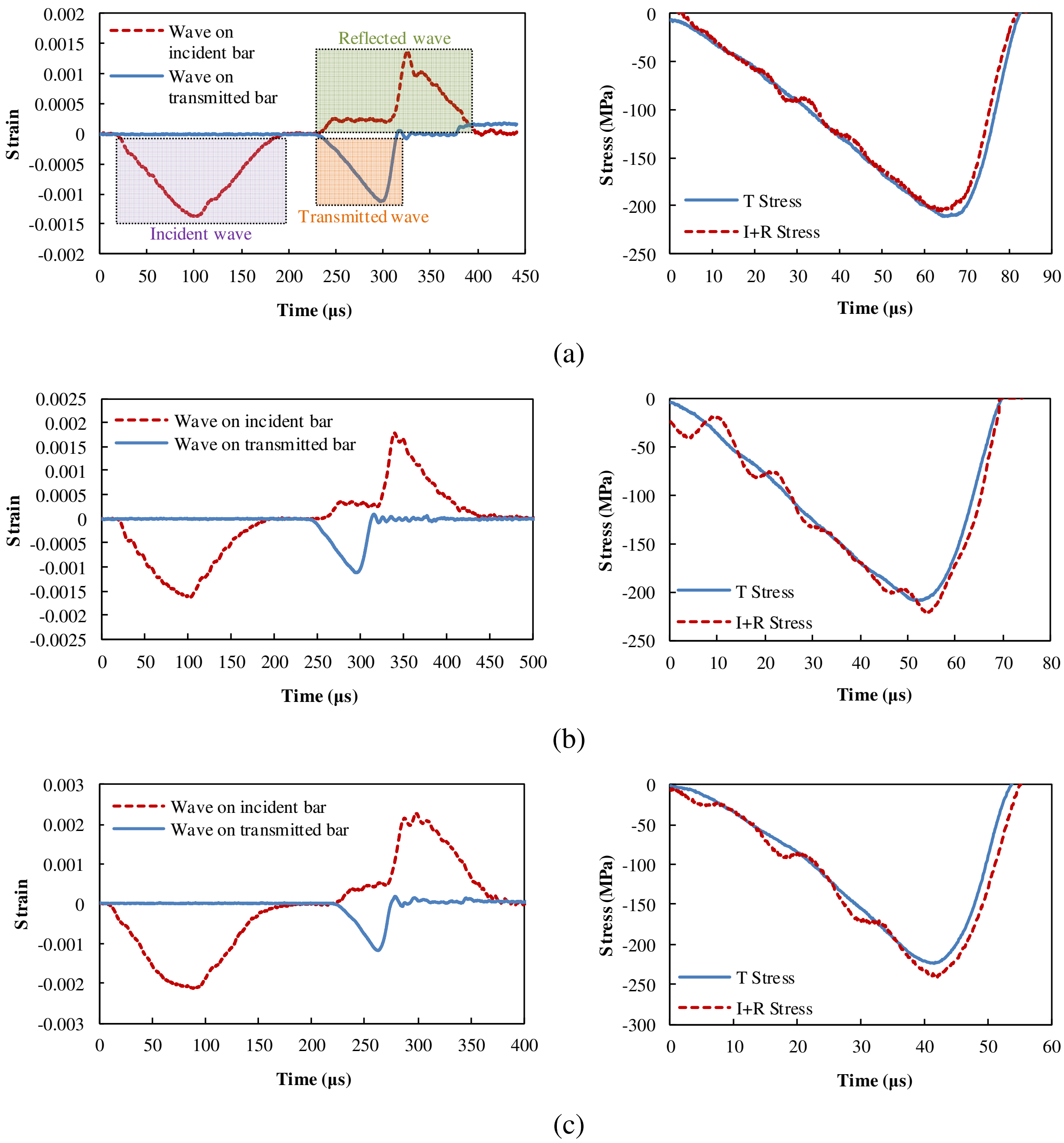

Fig. 12 Typical strain time-histories and dynamic equilibrium from the dynamic compressive tests: (a) DC-A-2, air pressure = 0.1 MPa, (b) DC-B-4, air pressure = 0.15 MPa and (c) DC-C-4, air pressure = 0.2 MPa

The Eng. stress-Eng. strain curves of the specimens from the tests with three different initial pressures are presented in Fig. 13. The Eng. stress was calculated by dividing the total force by the original sectional area of the specimen. The force acted on the end of specimen can be calculated by either Eq. 2 (based on the incident wave and reflected wave) or Eq. 3 (based on the transmitted wave) since good dynamic equilibrium was achieved. Here, the transmitted wave was used due to a higher signal-to-noise ratio. The Eng. strain was measured by the strain gauges attached on the specimen. The corresponding mechanical parameters were determined similarly to the static tests and are summarized in Table 6. Under dynamic loading, the LIFG also display an almost linear elastic behaviour before reaching the ultimate strength. However, unlike the quasi-static situation where the peak stress point in the stress-strain curve marks the ultimate and brittle failure, the stress-strain curves of LIFG under dynamic compression tend to exhibit a short but noticeable descending phase after the peak stress point. This dynamic phenomenon may be attributed to the fact that fracture of glass is not instantaneous, and comparing to the timescale of the dynamic loading the fracture process time is not negligible.

Table 6 Test results from dynamic compressive tests

Specimen No.	Approx. air pressure (MPa)	Thickness (mm)	Diameter (mm)	$\dot{\varepsilon}$ (s^{-1})	Ultimate strength f_{dyc} (MPa)	Strain at peak point	Ultimate strain ε_{dyc}	Elastic modulus E_{dyc} (GPa)
DC-A-1	0.1	7.96	5.4	245	1242	1.96%	2.12%	65.00
DC-A-2		8	5.4	301	1185	1.94%	2.33%	58.51
DC-A-3		7.94	5.36	240	1192	2.03%	2.20%	61.74
DC-A-4		7.94	5.4	257	1326	2.09%	2.19%	65.79
DC-A-5		7.94	5.4	335	1233	2.08%	2.43%	63.64
DC-B-1	0.15	7.98	5.42	493	1173	2.22%	2.51%	58.27
DC-B-2		7.98	5.38	-	1213	-	-	-
DC-B-3		7.98	5.4	302	1023	1.92%	2.24%	57.11
DC-B-4		7.98	5.4	417	1228	1.73%	2.01%	74.77
DC-C-1	0.2	7.96	5.38	491	1194	1.92%	2.27%	76.14
DC-C-2		7.96	5.4	433	1398	2.04%	2.43%	69.32
DC-C-3		7.94	5.4	670	1290	2.14%	2.43%	58.03
DC-C-4		7.94	5.42	453	1330	2.09%	2.40%	66.31
DC-C-5		7.94	5.4	560	1186	2.05%	2.46%	69.36
DC-C-6		8.04	5.4	656	1203	1.81%	2.07%	72.89
DC-C-7		8	5.4	750	1259	2.13%	2.47%	70.03

Note: The ultimate strength corresponds to the peak point, and the ultimate strain corresponds to the failure point.

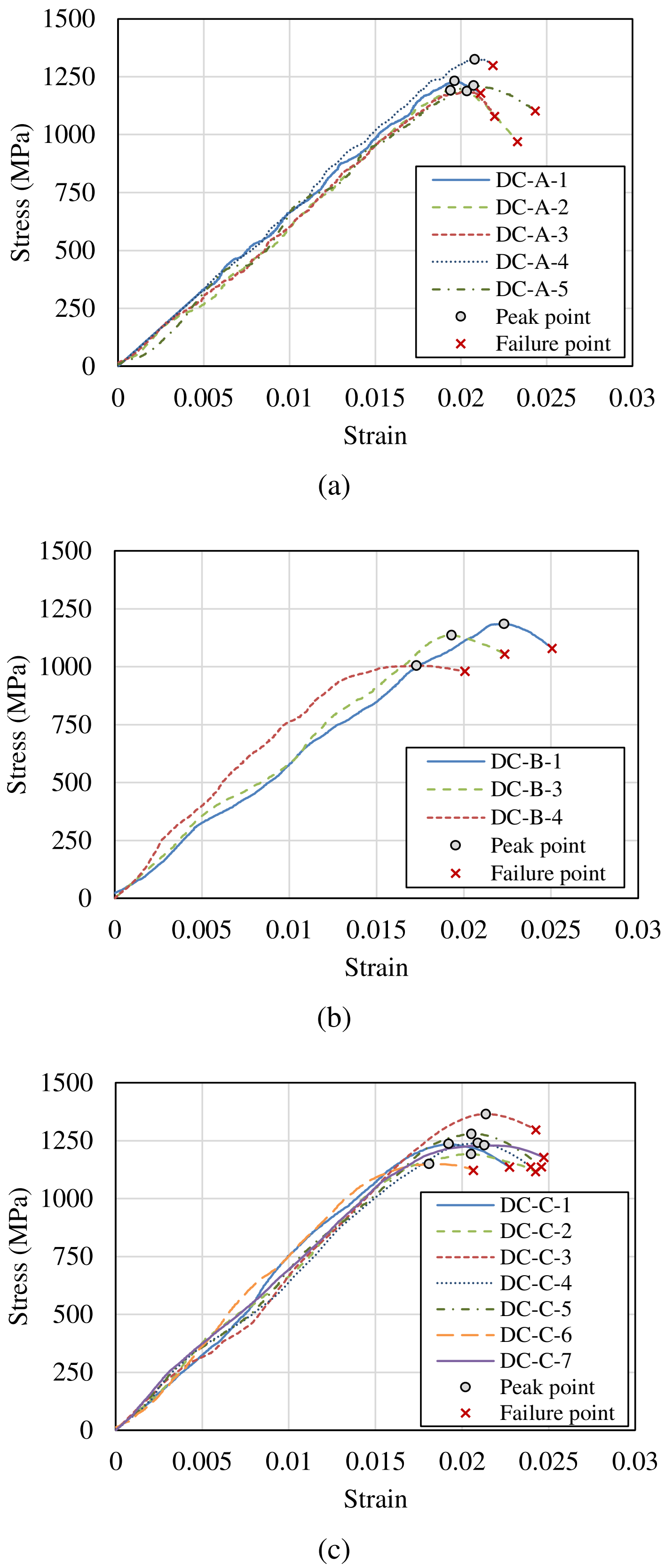

Fig. 13 Stress-strain curves from the dynamic compressive tests: (a) air pressure = 0.1 MPa, (b) air pressure = 0.15 MPa and (c) air pressure = 0.2 MPa

3.2.2 Dynamic splitting tensile test

Fig. 14a depicts a glass fracture process of a representative splitting test with an initial pressure of 0.03 MPa, and the corresponding loads/moments are marked in the stress time-history for comparison. As can be observed, the glass disc was compressed slightly when the stress wave went through. Longitudinal crack initiated from the central area of the glass at 190 μs, from a position around 3.5 mm away from the central line. From this point, the stress time-history becomes noticeably curved due to material damage. The crack quickly propagates towards the specimen-bar contact points at both ends. Finally, the glass cylinder was split and crushed. Similar process can be observed for dynamic splitting tests with an initial pressure of 0.05 MPa (Fig. 14b). It is worth noting that we also made attempts with higher impact velocities in order to realize higher strain rates. Fig. 14c shows the fracture process of a dynamic splitting test with an initial pressure of 0.09 MPa. It is observed that the specimen is fractured due to local crushing around the contact points at 170 μs, which leads to a sudden decline in the stress time-history. Although the specimen finally split into two or three halves, the failure of specimen initiated due to local crushing at the loading ends rather than splitting. The pressure of 0.05 MPa corresponds to a strain rate of around 35 s^{-1}, which is the highest strain rate achieved in the dynamic splitting tests in this study.

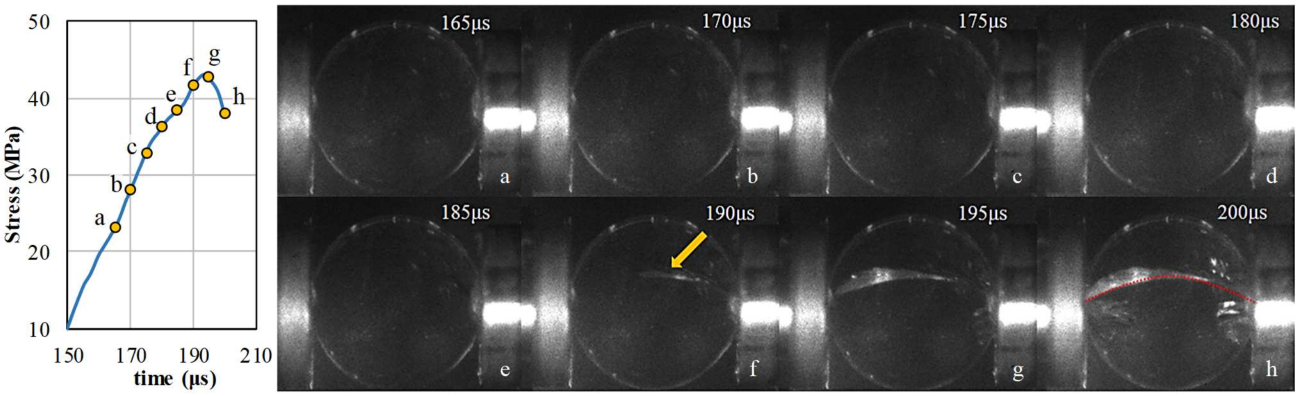

(a)

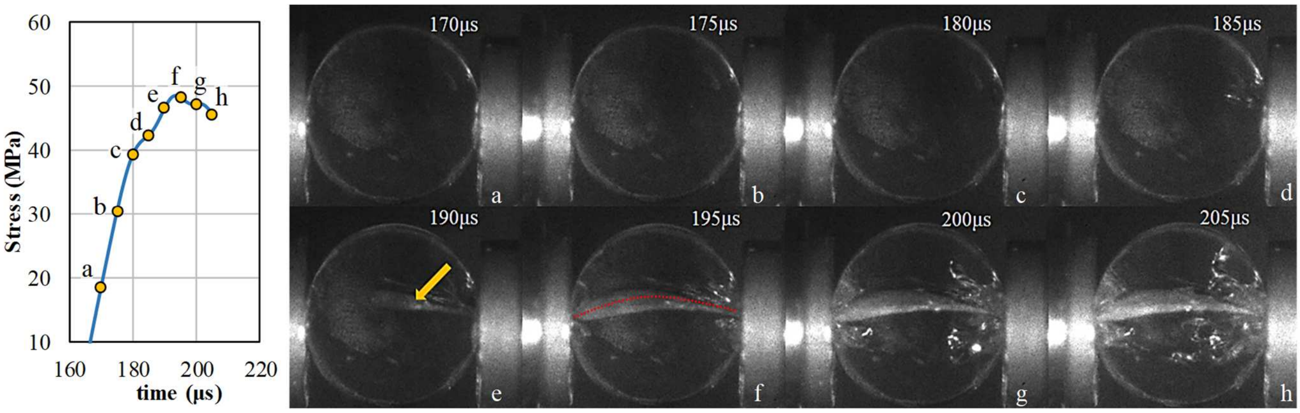

(b)

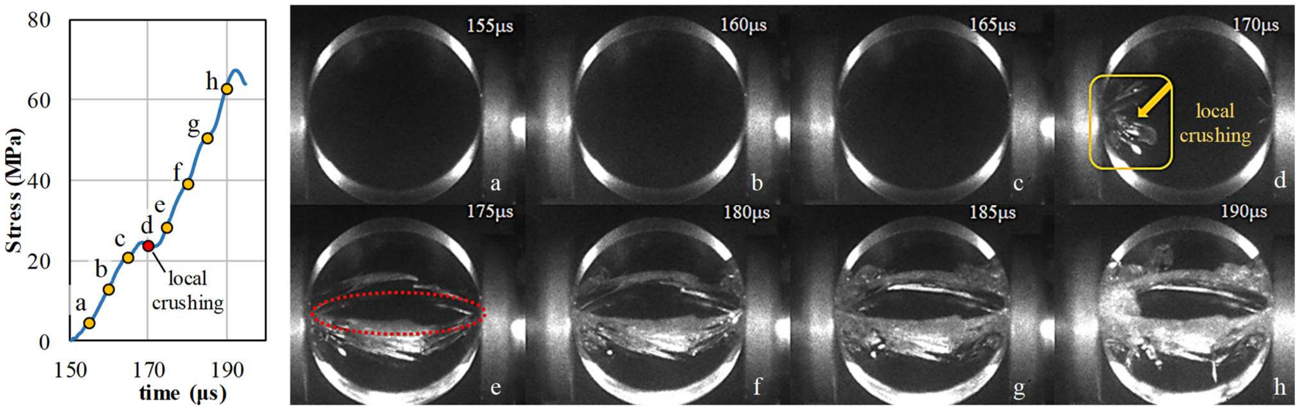

(c)

Fig. 14 Typical fracture process in dynamic splitting tests: (a) DS-A-1, initial pressure = 0.03 MPa, (b) DS-B-1, initial pressure = 0.05 MPa and (c) initial pressure = 0.09 MPa

Fig. 15 presents the results from the strain gauges on both incident and transmitted bars. The stress was calculated by multiplying the strain with the Young's modulus and the cross-section area of each bar. It can be observed that the values of σ_i+σ_r and σ_t gradually converge after the obvious initial oscillations, indicating the stress equilibrium was successfully realized in the specimen over a short period with the appropriate copper pulse shaper.

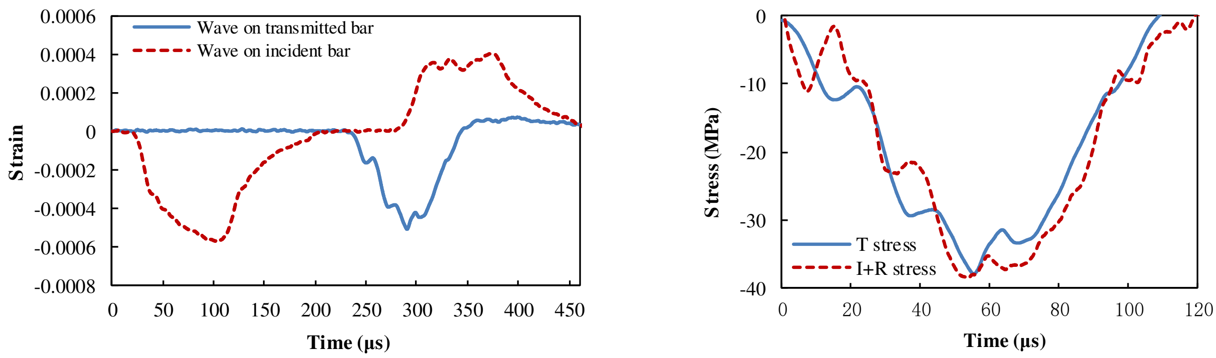

(a)

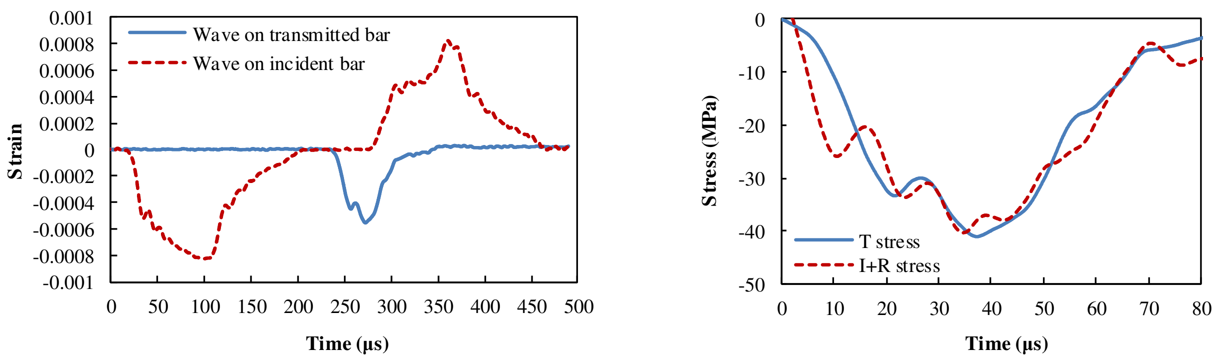

(b)

Fig. 15 Typical waveforms and dynamic equilibrium for dynamic splitting tensile tests: (a) DS-A-4, air pressure = 0.03 MPa and (b) DS-B-4, air pressure = 0.05 MPa

The Eng. stress-Eng. strain curves of the specimens from the dynamic splitting tests are presented in Fig. 16, and the corresponding mechanical parameters are summarized in Table 7. The Eng. stress was calculated by Eq. 1 and Eq. 3 based on the strain measured from the transmitted bar, while the

Eng. strain was measured by the strain gauges attached on the specimen. It can be found that the glass behaves nearly linear elastically before fracture and the failure is very brittle. Similar to the observations from the dynamic compressive tests, the specimen can still deform before it is totally fractured, resulting in a short descending phase in the stress-strain curve. Based on the results, it can be clearly observed that a higher strain rate will lead to an increase in the ultimate strength and slight increase in the tensile modulus. The strain rate effect is insignificant on the ultimate strain.

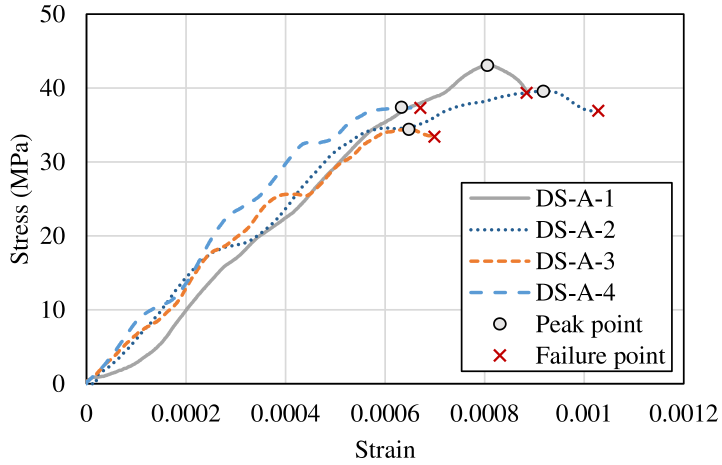

(a)

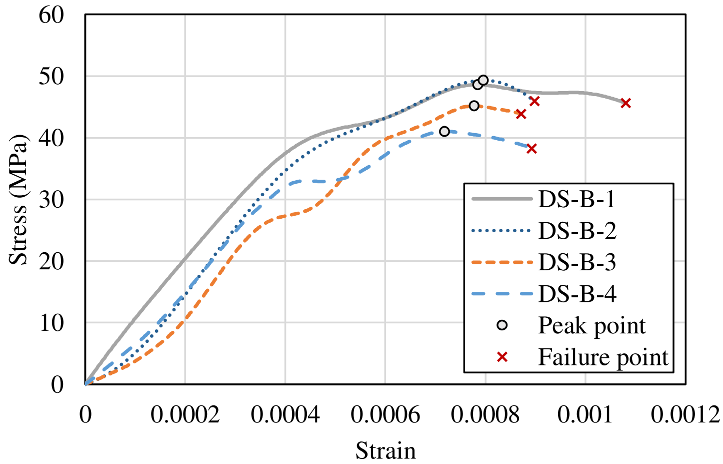

(b)

Fig. 16 Stress-strain curves for dynamic splitting tests: (a) air pressure = 0.03 MPa and (b) air pressure = 0.05 MPa

Table 7 Test results for dynamic splitting tests

Specimen No.	Approx. air pressure (MPa)	Thickness (mm)	Diameter (mm)	Strain Rate $\dot{\varepsilon}$ (s^{-1})	Ultimate strength f_{dyt} (MPa)	Strain at peak point	Ultimate strain ε_{dyt}	Elastic modulus E_{dyt} (GPa)
DS-A-1	0.03	9.21	19.94	20.6	43.11	0.081%	0.088%	58.01
DS-A-2		9.16	19.98	23.1	39.59	0.092%	0.103%	61.11
DS-A-3		9.20	19.98	16.8	34.44	0.065%	0.070%	57.81
DS-A-4		9.22	19.93	25.7	37.41	0.063%	0.067%	66.11
DS-B-1	0.05	9.14	19.92	36.4	48.60	0.078%	0.108%	61.98
DS-B-2		9.18	19.92	37.9	49.31	0.080%	0.090%	66.90
DS-B-3		9.28	19.96	29.5	45.19	0.078%	0.087%	69.14
DS-B-4		9.24	19.92	22.0	41.04	0.072%	0.089%	72.34

Note: The ultimate strength corresponds to the peak point, and the ultimate strain corresponds to the failure point.

4. Discussion on the strain rate effect

4.1 Strain rate limits for LIFG tests

As is introduced in section 3.1, the methods used to process the data from a typical SHPB test relies on the assumption of mechanical balance of the sample, i.e., a stress equilibrium state has to be achieved within a short time comparing to the time to fracture. Accordingly, the strain rate is limited as [26, 27],

$$T_e = n\frac{2l}{c_0} < T_{\mathrm{f}} = \frac{\varepsilon_f}{\bar{\dot{\varepsilon}}} \tag{6}$$

where T_e and T_{f} are the time needed to reach stress equilibrium and the time to fracture, respectively, ε_f is the ultimate strain of specimen, $\bar{\dot{\varepsilon}}$ is the average strain rate, l is the length of sample, c_0 is the wave speed and which equals to $c_0 = \sqrt{E/\rho}$, and n is the number of round-trips. Usually, the dynamic stress equilibrium can be achieved after at least 3~4 round-trips of the stress wave [28].

Here, we assume 3 wave round-trips in the specimen before fracture, the upper limits of the strain rate in dynamic compressive and splitting tensile tests can be determined as the following equations,

For dynamic compressive test: $$\bar{\dot{\varepsilon}}_{limit} = \frac{\varepsilon_f}{n\frac{2l}{\sqrt{E/\rho}}} = \frac{2.29\%}{3\times\frac{2\times 8mm}{\sqrt{(65.49\ GPa)/(2530\ kg\cdot m^{-3})}}} \approx 2480\ s^{-1} \tag{7a}$$

For dynamic splitting tensile test: $$\bar{\dot{\varepsilon}}_{limit} = \frac{\varepsilon_f}{n\frac{2l}{\sqrt{E/\rho}}} = \frac{0.09\%}{3\times\frac{2\times 20\ mm}{\sqrt{(64.06\ GPa)/(2530\ kg\cdot m^{-3})}}} \approx 40\ s^{-1} \tag{7b}$$

The above calculation indicates that the strain rate limit for dynamic compression test of LIFG using a SHPB setup is about 2500 s^{-1}, and that for dynamic splitting tensile test is about 40 s^{-1}. Obviously, the limits will depend upon the size of the sample: an increase of the length (for compression) or the diameter (for splitting) of the specimen from the 8 mm (for compression) or the 20 mm (for splitting) used in the present study will decrease the strain limits from the above values, and vice versa. Any attempt to push the strain rates above these limits may result in invalid test results either because of premature failure or a non-uniform stress distribution at fracture. In the current tests, the failure process as well as the stress equilibrium state were carefully checked to ensure the validity of the test results. Note that a maximum strain rate of around 40 s^{-1} was achieved in the splitting tensile tests, and higher tensile strain rates were found to result in local premature failure at the edges (Fig. 14c), which echoes the above conceptual analysis.

4.2 Ultimate strength

It is generally understood that the dominant failure mechanism of brittle (or quasi-brittle) materials, such as concrete, ceramics and glass, involves crack initiation, propagation, interaction and coalescence. Due to micro-inertia effects associated with the limited propagating speed of cracks, the process for the crack to open and grow is inhibited (or delayed) when the stress increases more rapidly than the crack propagation, leading to a retarded crack opening process and an increased failure strength [29-31]. On the other hand, multiple cracks of different sizes are driven simultaneously at a higher loading speed and higher stress level, which results in a significant reduction in the size of fragment as well as a higher material strength as compared to quasi-static loading.

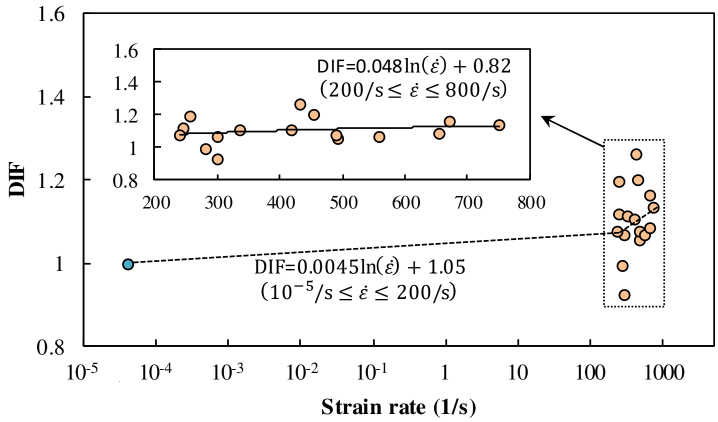

(a)

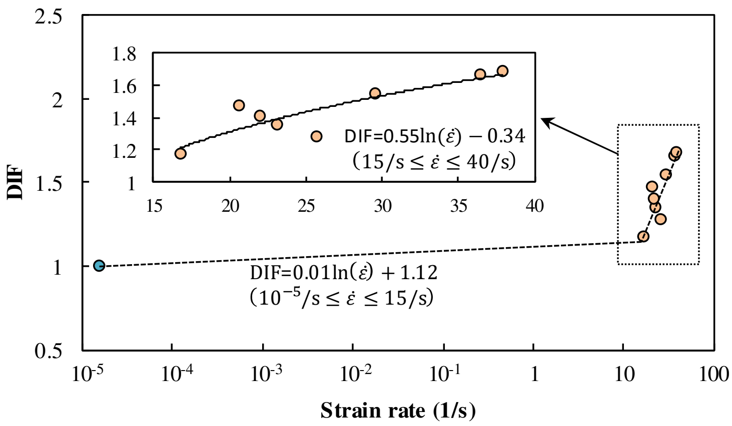

(b)

Fig. 17 Dynamic increase factors (DIFs) for the LIFG: (a) compressive strength and (b) tensile strength

In order to further quantify the strain rate effects on the dynamic strength of the LIFG from the tests, the dynamic increase factors (DIFs) were determined by normalizing the dynamic strengths with the averaged static strength. The obtained DIFs for both compression and splitting tension are plotted against the strain rates in Fig. 17. For the compressive strength, a clear trend of gradual increase in the DIF with respect to strain rate can be observed. The compressive strength of the LIFG increases by about 10% at strain rate of 250 s^{-1}, and the increment is about 20% when strain rate reaches 750 s^{-1}. On the other hand, more significant strain rate effect can be observed in the tensile strength. While the tensile strength only shows a slight increase at the low strain rate range, a rapid increase occurs when the strain rate exceeds 10 s^{-1}. As a representation, the tensile DIF is about 1.6 at strain rate of 35 s^{-1}. The comparison indicates that the tensile strength of the LIFG has a much stronger strain rate sensitivity than the compressive strength. This could be partially due to the fact that the compression failure is not governed by the opening of cracks and therefore is less affected by micro-inertia.

The DIFs obtained from the present tests are further compared with the data reported in other studies [2, 6, 13, 18, 32-34], as shown in Fig. 18. For compressive DIFs, the results from Holmquist et al. [2] (for NFG) and Peroni et al. [6] (for LIFG) are included, and the reported average static compressive strengths are 1022.5 MPa (from 4 repeated tests) and 1087.8 MPa (from 5 repeated tests), respectively, which are comparable to the LIFG used in this study. As shown in Fig. 18a, the obtained DIFs show good agreement with the other published results and indicates that the compressive strength does not show significant strain rate effect within the strain rate range from 10^2 s^{-1} to 10^3 s^{-1}. It should be mentioned that Zhang et al. [7] has also conducted dynamic compressive tests on the NFG, from which the compressive DIFs were found to be around 1.5-3 over a strain rate range from 100 s^{-1} to 380 s^{-1}, showing a stronger strain rate sensitivity. This could be mainly attributed to the difference in the chemical composition. As listed in Table 1, the glass used in Zhang's tests has a noticeable lower SiO_2

percentage of 51% compared to 72~74% in other studies, which leads to a much lower strength[7]. Therefore, it is more likely that lower strength NFG may exhibit higher DIF and more significant strain rate sensitivity.

On the other hand, extensive studies were carried out to determine the tensile strength of float glass since it's more important in structural application. However, most studies are concerned with quasi-static loading and low to intermediate strain rate cases, and very limited data can be found when considering higher strain rates. It is worth noting that the results presented in Fig. 18b were determined through different experimental method, including three-point bending tests [32, 33], uniaxial tensile tests using universal high-speed testing machine [34], and compression/splitting tensile tests [6] or double-ring bending tests [13, 18] using SHPB facilities. Though the results show a considerable variation, especially in high strain rate levels, a significant strain rate effect can be observed when the strain rate is above 10^0 s^{-1}.

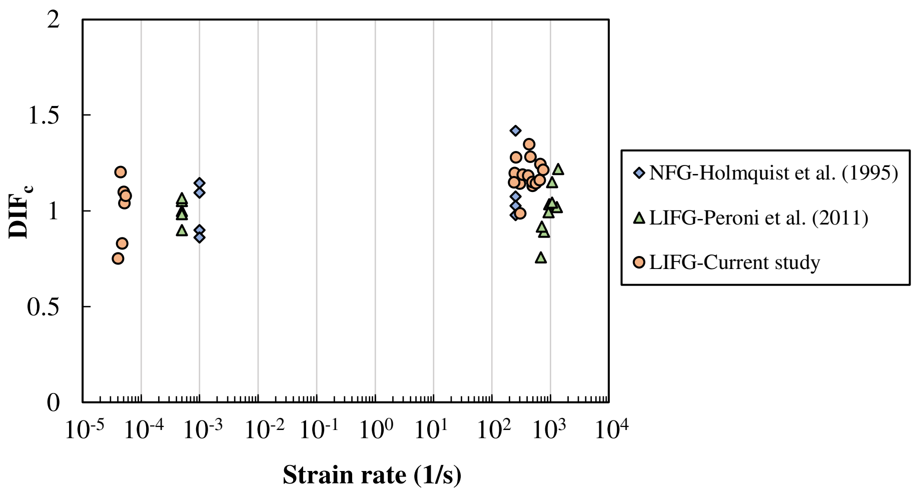

(a)

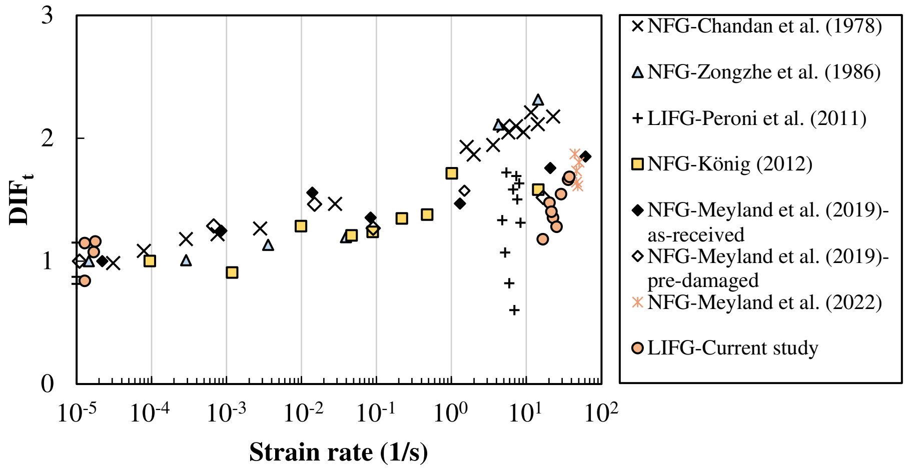

(b)

Fig. 18 Comparison of the DIFs for the float glass: (a) compressive DIFs and (b) tensile DIFs

4.3 Ultimate strain

Strain rate also has notable influences on the ultimate compressive and tensile strains of the LIFG. As can be seen in Fig. 19, the average ultimate compressive strain of the LIFG is around 2.3% over the strain rate range of 250-750 s^{-1}, which is around 30% larger than the static ultimate compressive strain. The average ultimate tensile strain of the LIFG is around 0.088% over the strain rate range of 15-40 s^{-1}, which is around 80% larger than the static ultimate tensile strain. Upon further checking of the fracture process of the glass specimens in the dynamic tests, it can be observed that the fracture of glass specimen is not instantaneous. In other words, the duration of glass fracture is not negligible compared with the loading duration. This could be evidenced by a short but notable descending phase in the stress at the end of the stress-strain curves (Fig. 13 and Fig. 16), which represents major cracks starting propagating inside the glass specimen before the glass is totally fractured. Therefore, the recorded ultimate strain may be overestimated.

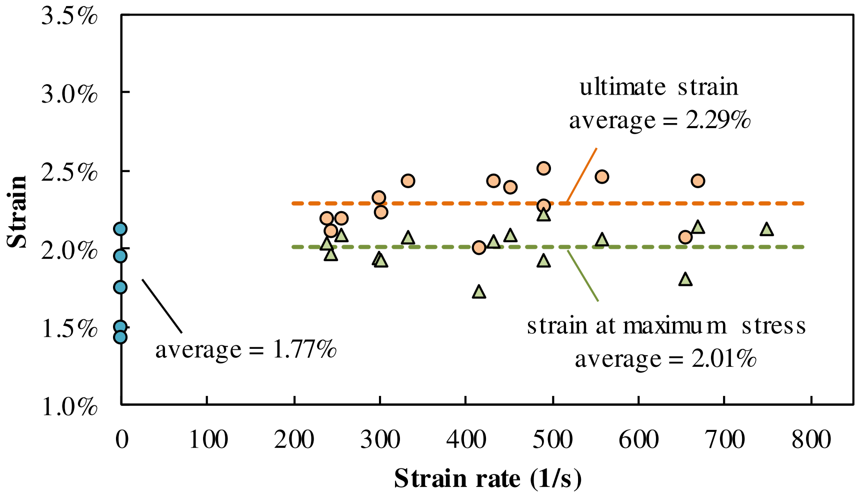

(a)

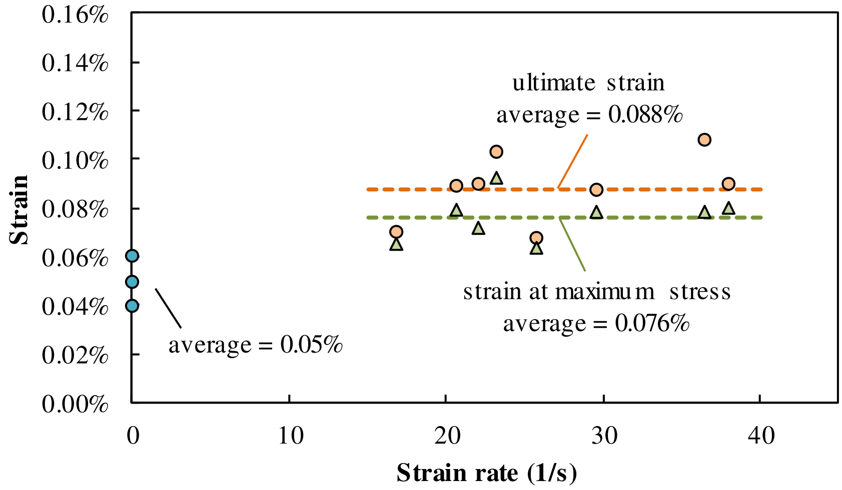

(b)

Fig. 19 Ultimate strains for the LIFG: (a) ultimate compressive strain and (b) ultimate tensile strain

The strain at the maximum stress (i.e., the peak point on the stress-strain curve) is also presented in Fig. 19 for comparison. It should be pointed out that the strain at the peak stress is about 10% smaller than the ultimate strain for the dynamic compressive or dynamic splitting tensile results, while there is essentially no difference between the peak and ultimate strains under quasi-static loading. The strain at the maximum stress increases with the strain rate for both compression and tension cases. The strain at the maximum stress increases by about 30% at the strain rate of 750 s^{-1} under compression, while it increases by about 50% at the strain rate of 40 s^{-1} under tension, indicating that the strain rate effect is more significant under tension.

4.4 **Elastic modulus**

Fig. 20 shows the Young's modulus obtained from the current tests as well as those from the open literatures [5-7, 13, 34, 35], based on which a general evaluation of the strain rate effects on the float glass is made. A considerable variation can be observed from all the test results, even within each single test group. The variation mainly results from different test methods employed and specimen conditions (e.g., glass type, surface/edge treatment). In general, the results from our study (average value ≈ 65 GPa) are comparable to the other results, and a little bit lower than the value suggested in the European Standard EN 572-1 [36], i.e., 70GPa. The strain rate effect is not significant on the Young's modulus of float glass over the strain range from 10^{-6} to 10^{5} s^{-1}.

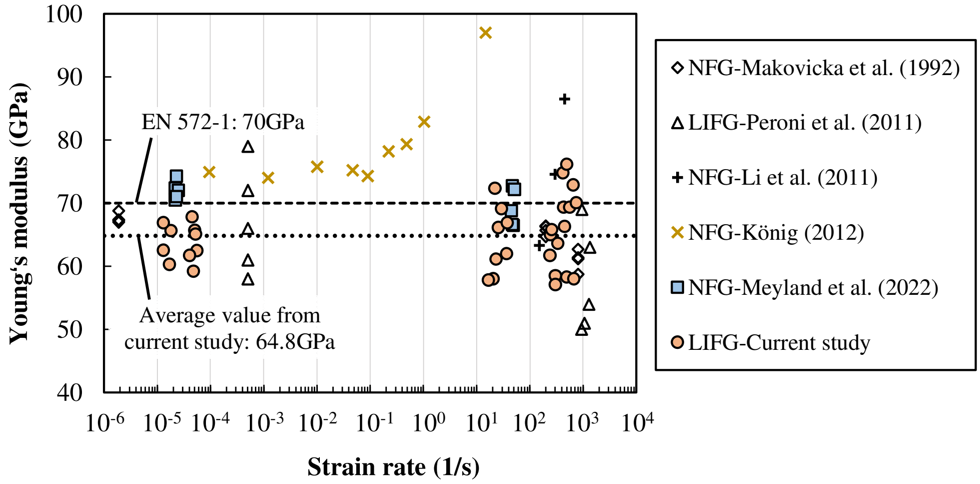

Fig. 20 Young's modulus for the LIFG: (a) compressive Young's modulus and (b) tensile Young's modulus

5. Conclusions

In this paper, the dynamic mechanical properties of LIFG have been studied through static and dynamic compressive and splitting tensile tests. Based on the test results, strain rate effects on key mechanical parameters of LIFG have been evaluated. The following main conclusions may be drawn:

1. The LIFG exhibits linear elastic behaviour under quasi-static compression and tension, and the corresponding average compressive modulus and tensile modulus are 65.49 GPa and 64.06 GPa, respectively, which are approximately the same. The average static compressive strength and splitting tensile strength of LIFG are around 1038 and 29 MPa, respectively. The splitting tensile strength is around 1/35 of its compressive strength, indicating significant tension-compression anisotropy. Similar phenomenon can also be observed in dynamic tests.

2. The dynamic tests using SHPB show that the strain rate effect on the strength of the LIFG is more significant in (splitting) tension than in compression. More specifically, the compressive strength of LIFG increases by about 20% over the strain rate rage of 10^{-5} to 750 s^{-1}, while the increment is 40% for splitting tensile strength over the strain rate range of 10^{-5} to 40 s^{-1}. The strain rate effect on the Young's modulus of LIFG is neglectable.

3. Unlike the quasi-static situation where the peak stress point in the stress-strain curve marks the ultimate and brittle failure, the stress-strain curves of LIFG under both dynamic compression and dynamic tension tend to exhibit a short but noticeable descending phase after the peak stress point. As a result, the ultimate compressive and tensile strains obtained from the dynamic tests are around 10% larger than those obtained from the static tests. This dynamic phenomenon may be attributed to the fact that fracture of glass is not instantaneous, and comparing to the timescale of the dynamic loading the fracture process time is not negligible.

4. Based on a conceptual analysis, the upper boundaries of strain rates that could be achieved in the dynamic compression and splitting tension using the traditional SHPG facilities for LIFG are estimated to be about 2500 s^{-1} and 40 s^{-1}, with a specimen dimension in the loading direction of 8 mm (for compression) or 20 mm (for splitting tension). The above limiting strain rates will decrease if the specimen dimension is increased, or otherwise increase if the specimen dimension is reduced. Testing at strain rates above the upper limits may result in invalid results either because of premature failure or a non-uniform stress distribution at fracture.

Acknowledgements

The authors gratefully acknowledge the financial support by the National Natural Science Foundation of China under the grant No. 51678448 and the State Key Laboratory for Disaster Reduction in Civil Engineering, Tongji University under the grant No. SLDRCE 19-B-18.

Reference

[1] Norville H S, Harvill N, Conrath E J, et al. Glass-related injuries in Oklahoma City bombing[J]. Journal of Performance of Constructed Facilities, 1999, 13(2): 50-56.

[2] Holmquist T J, Johnson G R, Lopatin C M, et al. High strain rate properties and constitutive modeling of glass[R]. Sandia National Lab.(SNL-NM), Albuquerque, NM (United States), 1995.

[3] Nie X, Chen W W, Sun X, et al. Dynamic failure of borosilicate glass under compression/shear loading experiments[J]. Journal of the American Ceramic Society, 2007, 90(8): 2556-2562.

[4] LI Lei, AN Er-feng, YANG Jun. Impact Properties of Typical Architectural Glass by SHPB [J]. Bulletin of the Chinese Ceramic Society, 2010, (2): 390-394. (in Chinese)

[5] LI Lei, AN Er-feng, YANG Jun. Strain Rate Dependent Dynamic Constitutive Equation of Float Glass [J]. Journal of Building Materials, 2011, 14(2): 202-206. (in Chinese)

[6] Peroni M, Solomos G, Pizzinato V, et al. Experimental investigation of high strain-rate behaviour of glass[C]//Applied mechanics and materials. Trans Tech Publications Ltd, 2011, 82: 63-68.

[7] Zhang X, Zou Y, Hao H, et al. Laboratory test on dynamic material properties of annealed float glass[J].

International Journal of Protective Structures, 2012, 3(4): 407-430.

[8] Zhang X, Hao H, Ma G. Dynamic material model of annealed soda-lime glass[J]. International Journal of Impact Engineering, 2015, 77: 108-119.

[9] Daryadel S S, Mantena P R, Kim K, et al. Dynamic response of glass under low-velocity impact and high strain-rate SHPB compression loading[J]. Journal of Non-Crystalline Solids, 2016, 432: 432-439.

[10] Sheikh M Z, Wang Z, Du B, et al. Static and dynamic Brazilian disk tests for mechanical characterization of annealed and chemically strengthened glass[J]. Ceramics International, 2019, 45(6): 7931-7944.

[11] Sheikh M Z, Zhen W, Tao S, et al. Dynamic failure of un-strengthened aluminosilicate glass[J]. Theoretical and Applied Fracture Mechanics, 2019, 104: 102325.

[12] Sheikh M Z, Atif M, Li Y, et al. Damage mechanisms and energy absorption of aluminosilicate glass under compression/tensile loading[J]. Construction and Building Materials, 2021, 288: 123088.

[13] Meyland M J, Nielsen J H. High strain rate characterisation of soda-lime-silica glass and the effect of residual stresses[J]. Glass Structures & Engineering, 2022: 1-17.

[14] Osnes K, Børvik T, Hopperstad O S. Testing and modelling of annealed float glass under quasi-static and dynamic loading[J]. Engineering fracture mechanics, 2018, 201: 107-129.

[15] Pisano G, Carfagni G R. The statistical interpretation of the strength of float glass for structural applications[J]. Construction and Building Materials, 2015, 98: 741-756.

[16] Castori G, Speranzini E. Fracture strength prediction of float glass: The coaxial double ring test method[J]. Construction and Building Materials, 2019, 225: 1064-1076.

[17] Ballarini R, Pisano G, Carfagni G R. New calibration of partial material factors for the structural design of float glass. Comparison of bounded and unbounded statistics for glass strength[J]. Construction and Building Materials, 2016, 121: 69-80.

[18] Meyland M J, Bønding C K T, Eriksen R N W, et al. An experimental investigation of the flexural strength of soda–lime–silica glass at high loading rates[J]. Glass Structures & Engineering, 2019, 4(2): 175-183.

[19] Meyland M J, Nielsen J H, Kocer C. Tensile behaviour of soda-lime-silica glass and the significance of load duration–A literature review[J]. Journal of Building Engineering, 2021, 44: 102966.

[20] American Society for Testing and Materials. Standard test method for splitting tensile strength of intact rock core specimens[S]. ASTM International, 2016.

[21] Muskhelishvili N I. Some basic problems of the mathematical theory of elasticity[M]. Groningen: Noordhoff, 1953.

[22] DING Rui, Researches on static and dynamic properties of float glass [D]. Tongji University (master thesis), 2011. (in Chinese)

[23] Gama B A, Lopatnikov S L, Gillespie Jr J W. Hopkinson bar experimental technique: a critical review[J]. Appl. Mech. Rev., 2004, 57(4): 223-250.

[24] Frew D J, Forrestal M J, Chen W. Pulse shaping techniques for testing brittle materials with a split Hopkinson pressure bar[J]. Experimental mechanics, 2002, 42(1): 93-106.

[25] Yu Y, Yin J, Zhong Z. Shape effects in the Brazilian tensile strength test and a 3D FEM correction[J]. International journal of rock mechanics and mining sciences, 2006, 4(43): 623-627.

[26] Forquin P, Riedel W, Weerheijm J. Dynamic test devices for analyzing the tensile properties of concrete[M]//Understanding the tensile properties of concrete. Woodhead Publishing, 2013: 137-181e.

[27] Lu Y. Modelling the dynamic response of concrete with mesoscopic heterogeneity[M]//Understanding the Tensile Properties of Concrete. Woodhead Publishing, 2013: 218-272e.

[28] GRAY III G T. Classic split Hopkinson pressure bar testing[J]. ASM handbook, 2000, 8: 462-476.

[29] Hai L, Wu J Y, Li J. A phase-field damage model with micro inertia effect for the dynamic fracture of quasi-brittle solids[J]. Engineering Fracture Mechanics, 2020, 225: 106821.

[30] WEERHEIJM J. Understanding the tensile properties of concrete[M]. Elsevier, 2013.

[31] Bavdekar S, Subhash G. Failure mechanisms of ceramics under quasi-static and dynamic loads: overview[J]. Handbook of damage mechanics, 2022: 579-607.

[32] Chandan H C, Bradt R C, Rindone G E. Dynamic fatigue of float glass[J]. Journal of the American Ceramic Society, 1978, 61(5-6): 207-210.

[33] Zongzhe J, Junarong M, Xiaorui L. Dynamic fracture and Strength of Glass[J]. Proceedings XIVth Int. Congr. on glass, 1986: 78-83.

[34] König C. Dehnratenabhängigkeit mechanischer Werkstoffkennwerte von Kalk-Natronsilicatglas[D]. Ph.d., Technischen Universität Carolo-Wilhelmina zu Braunschweig, 2012.

[35] Makovička D, Lexa P. Dynamic response of window glass plates under explosion overpressure[C]//Structures Under Shock and Impact II: Proceedings of the Second International Conference, held in Portsmouth, UK, 16th–18th June, 1992. Thomas Telford Publishing, 1992: 381-392.

[36] DIN EN 572-1. Glass in Building–Basic Soda Lime Silicate Glass Products–Part 1: Definitions and General Physical and Mechanical Properties[J]. 2012.